Observation of $\pi^- K^+$ and $\pi^+ K^-$ Atoms

B. Adeva,[1] L. Afanasyev,[2] Y. Allkofer,[3] C. Amsler,[4] A. Anania,[5] S. Aogaki,[6] A. Benelli,[7] V. Brekhovskikh,[8] T. Cechak,[7] M. Chiba,[9] P. Chliapnikov,[8] P. Doskarova,[7] D. Drijard,[10] A. Dudarev,[2] D. Dumitriu,[6] D. Fluerasu,[6] A. Gorin,[8] O. Gorchakov,[2] K. Gritsay,[2] C. Guaraldo,[11] M. Gugiu,[6] M. Hansroul,[10] Z. Hons,[12] S. Horikawa,[3] Y. Iwashita,[13] V. Karpukhin,[2] J. Kluson,[7] M. Kobayashi,[14] V. Kruglov,[2] L. Kruglova,[2] A. Kulikov,[2] E. Kulish,[2] A. Kuptsov,[2] A. Lamberto,[5] A. Lanaro,[15] R. Lednicky,[16] C. Mariñas,[1] J. Martincik,[7] L. Nemenov,[2,10] M. Nikitin,[2] K. Okada,[17] V. Olchevskii,[2] M. Pentia,[6] A. Penzo,[18] M. Plo,[1] P. Prusa,[7] G. Rappazzo,[5] A. Romero Vidal,[11] A. Ryazantsev,[8] V. Rykalin,[8] J. Saborido,[1] J. Schacher,[4,*] A. Sidorov,[8] J. Smolik,[7] F. Takeutchi,[17] L. Tauscher,[19] T. Trojek,[7] S. Trusov,[20] T. Urban,[7] T. Vrba,[7] V. Yazkov,[20] Y. Yoshimura,[14] M. Zhabitsky,[2] and P. Zrelov[2]

(DIRAC Collaboration)

[1]*Santiago de Compostela University, Santiago de Compostela, Spain*
[2]*JINR, Dubna, Russia*
[3]*Zurich University, Zurich, Switzerland*
[4]*Albert Einstein Center for Fundamental Physics, Laboratory of High Energy Physics, Bern, Switzerland*
[5]*INFN, Sezione di Trieste and Messina University, Messina, Italy*
[6]*IFIN-HH, National Institute for Physics and Nuclear Engineering, Bucharest, Romania*
[7]*Czech Technical University in Prague, Prague, Czech Republic*
[8]*IHEP, Protvino, Russia*
[9]*Tokyo Metropolitan University, Tokyo, Japan*
[10]*CERN, Geneva, Switzerland*
[11]*INFN, Laboratori Nazionali di Frascati, Frascati, Italy*
[12]*Nuclear Physics Institute ASCR, Rez, Czech Republic*
[13]*Kyoto University, Kyoto, Japan*
[14]*KEK, Tsukuba, Japan*
[15]*University of Wisconsin, Madison, USA*
[16]*Institute of Physics ASCR, Prague, Czech Republic*
[17]*Kyoto Sangyo University, Kyoto, Japan*
[18]*INFN, Sezione di Trieste, Trieste, Italy*
[19]*Basel University, Basel, Switzerland*
[20]*Skobeltsin Institute for Nuclear Physics of Moscow State University, Moscow, Russia*

(Received 28 May 2016; published 8 September 2016)

The observation of hydrogenlike πK atoms, consisting of $\pi^- K^+$ or $\pi^+ K^-$ mesons, is presented. The atoms are produced by 24 GeV/c protons from the CERN PS accelerator, interacting with platinum or nickel foil targets. The breakup (ionization) of πK atoms in the same targets yields characteristic πK pairs, called "atomic pairs," with small relative momenta Q in the pair center-of-mass system. The upgraded DIRAC experiment observed 349 ± 62 such atomic πK pairs, corresponding to a signal of 5.6 standard deviations. This is the first statistically significant observation of the strange dimesonic πK atom.

DOI: 10.1103/PhysRevLett.117.112001

Introduction.—A first investigation of the πK atom was performed by means of a platinum target at the CERN PS accelerator with 24 GeV/c protons in 2007 [1,2]. [The term πK atom or $A_{K\pi}$ refers to $\pi^- K^+$ and $\pi^+ K^-$ atoms.] An enhancement of πK pairs at low Q was observed, corresponding to 173 ± 54 πK atomic pairs or a significance of 3.2 standard deviations (σ). [The quantity Q denotes the experimental relative momentum in the pair c.m. system. The longitudinal (Q_L) and transverse ($Q_T = \sqrt{Q_X^2 + Q_Y^2}$) components of the vector $\vec{Q}$ are defined with respect to the direction of the total laboratory (lab) pair momentum.] In the experiment from 2008 to 2010, DIRAC detected an excess of 178 ± 49 πK pairs in a Ni target, an effect of only $3.6\,\sigma$ [3]. In the present Letter, experimental data obtained in Ni and Pt targets were analysed, using recorded information from all detectors and an enhanced

background description based on Monte Carlo (MC) simulations. The correction of the setup geometry, the simulation of the detector response, the background suppression, and the admixture evaluation were significantly improved for the whole running period. These improvements allow a statistically reliable πK atom observation for the first time.

Meson-meson interactions at low energy are the simplest hadron-hadron processes and allow us to test low-energy QCD, specifically chiral perturbation theory [4–7]. The observation and the measurement of the $\pi^+\pi^-$ atom (pionium) lifetime were reported in Refs. [8–10]. Going one step further, the observation and the lifetime measurement of the πK atom involving strangeness provides a direct determination of a difference of basic S-wave πK scattering lengths [11]. This atom is an electromagnetically bound πK state with a Bohr radius of $a_B = 249$ fm and a binding energy (ground state) of $E_B = 2.9$ keV. It decays predominantly by strong interaction into two neutral mesons $\pi^0 K^0$ or $\pi^0 \bar{K}^0$. The decay width $\Gamma_{\pi K}$ in the ground state ($1S$) is given by the relation [11,12] $\Gamma_{\pi K} = (1/\tau) = R(a_0^-)^2$, where $a_0^- = \frac{1}{3}(a_{1/2} - a_{3/2})$ is the S-wave isospin-odd πK scattering length (a_I is the πK scattering length for isospin I) and R is a precisely known factor (relative precision 2%). The scattering length a_0^- was studied in chiral perturbation theory [13–15], in the dispersive framework [16], and in lattice QCD (see, e.g., Ref. [17]). Using a_0^- from Ref. [16], one predicts for the πK atom lifetime $\tau = (3.5 \pm 0.4) \times 10^{-15}$ s.

A method to produce and observe hadronic atoms was developed [18]. In the DIRAC experiment, relativistic dimesonic bound states, formed by Coulomb final state interaction (FSI), are moving inside the target and can break up: the resulting atomic pairs (Fig. 1) have $Q < 3$ MeV/c.

Setup.—The setup [19], sketched in Fig. 2, detects and identifies $\pi^+\pi^-$, $\pi^- K^+$, and $\pi^+ K^-$ pairs with small Q. The structure of these pairs after the magnet is approximately symmetric for $\pi^+\pi^-$ and asymmetric for πK. Originating from a bound system, these particles travel with nearly the same velocity, and hence for πK atomic pairs the kaon momentum is by a factor of about $(M_K/M_\pi) \approx 3.5$ larger than the pion momentum (M_K is the charged kaon mass and M_π the charged pion mass). The two-arm vacuum magnetic spectrometer is optimized for simultaneous detection of these pairs [20].

The 24 GeV/c primary proton beam, extracted from the CERN PS accelerator, hit a (26 ± 1) μm thick Pt target in 2007 (the Pt target maximizes the production of atomic pairs) and Ni targets with thicknesses (98 ± 1) μm in 2008 and (108 ± 1) μm in 2009 and 2010 (the Ni targets are optimal for the lifetime measurement). The radiation thickness of the 98 (108) μm Ni target amounts to about 7×10^{-3} X_0 (radiation length).

The secondary channel (solid angle $\Omega = 1.2 \times 10^{-3}$ sr) together with the whole setup is vertically inclined relative

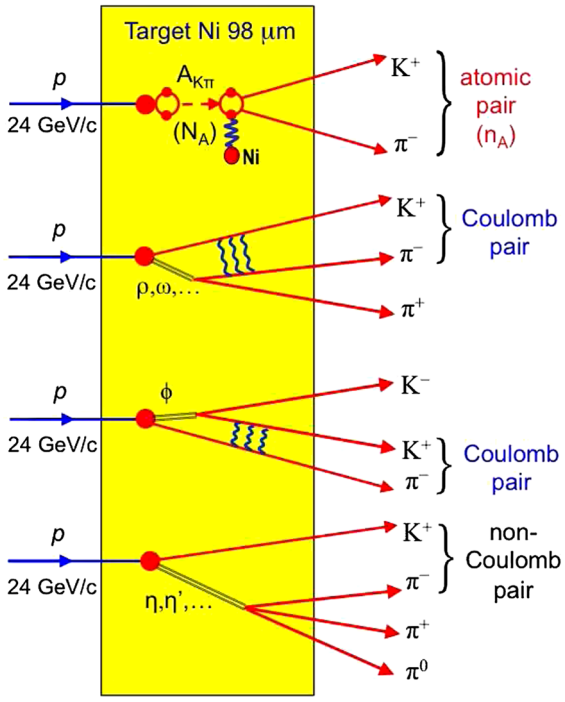

FIG. 1. Inclusive πK production in the 24 GeV/c p-Ni interaction $p + \mathrm{Ni} \to \pi^- K^+ + X$. The ionization or breakup of $A_{K\pi}$ leads to atomic pairs. (For more details, see the text in the section entitled "Bound and free πK pair production.")

to the proton beam by 5.7° upward. Secondary particles propagate mainly in vacuum up to the Al foil at the exit of the vacuum chamber, which is located between the poles of the dipole magnet ($B_{\max} = 1.65$ T and $BL = 2.2$ T m). In the vacuum gap, microdrift chambers (MDC) with 18 planes and the scintillating fiber detector (SFD) with three planes X, Y, and U inclined by 45° were installed to measure the particle coordinates ($\sigma_{\mathrm{SFD}x} = \sigma_{\mathrm{SFD}y} = 60$ μm,

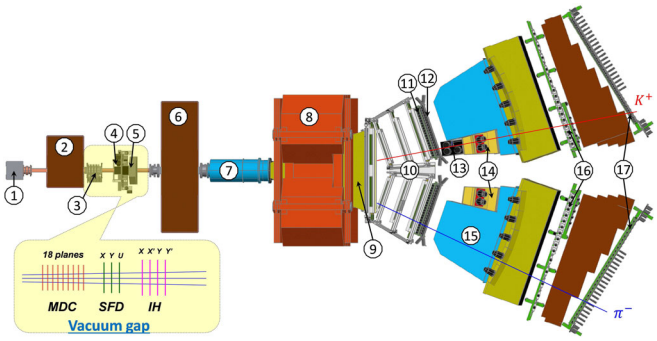

FIG. 2. General view of the DIRAC setup. 1: target station. 2: first shielding wall. 3: microdrift chambers. 4: scintillating fiber detector. 5: ionization hodoscope. 6: second shielding wall. 7: vacuum tube. 8: spectrometer magnet. 9: vacuum chamber. 10: drift chambers. 11: vertical hodoscope. 12: horizontal hodoscope. 13: aerogel Cherenkov counter. 14: heavy gas Cherenkov counter. 15: nitrogen Cherenkov counter. 16: preshower. 17: muon detector.

$\sigma_{\mathrm{SFD}u} = 120\ \mu$m) and particle time ($\sigma_{t\mathrm{SFD}x} = 380$ ps, $\sigma_{t\mathrm{SFD}y} = \sigma_{t\mathrm{SFD}u} = 520$ ps). Furthermore, the four planes of the scintillation ionization hodoscope (IH) serve to identify unresolved double track events with only one hit in the SFD. Each spectrometer arm is equipped with the following subdetectors: drift chamber (DC) to measure the particle coordinates with about 85 μm precision, a vertical hodoscope (VH) to measure time with 110 ps accuracy for triggering and particle identification via time-of-flight determination, a horizontal hodoscope (HH) to select pairs with a vertical separation less than 75 mm between the arms (that cuts $Q_Y < 15$ MeV/c), an aerogel Cherenkov counter (ChA) to distinguish kaons from protons, a heavy gas (C_4F_{10}) Cherenkov counter (ChF) to distinguish pions from kaons; a nitrogen Cherenkov counter (ChN) and a preshower detector to identify e^+e^- pairs, an iron absorber, and a two-layer scintillation counter to identify muons. In the "negative" arm, an aerogel counter was not installed, because the number of antiprotons is small compared to K^-.

Pairs of oppositely charged time-correlated particles (prompt pairs) and accidentals in the time interval ± 20 ns are selected by requiring a two-arm coincidence (ChN in anticoincidence) with the coplanarity restriction (HH) in the first-level trigger. The second-level trigger selects events with at least one track in each arm by exploiting the DC-wire information (track finder). Using the track information, the online trigger selects $\pi\pi$ and πK pairs with relative momenta $|Q_X| < 12$ MeV/c and $|Q_L| < 30$ MeV/c. The trigger efficiency is about 98% for pairs with $|Q_X| < 6$ MeV/c, $|Q_Y| < 4$ MeV/c, and $|Q_L| < 28$ MeV/c. Particle pairs $\pi^- p$ ($\pi^+\bar{p}$) from Λ ($\bar{\Lambda}$) decay were used for the calibration of the spectrometer and e^+e^- pairs for general detector calibration.

Bound and free πK pair production.—Prompt $\pi^\mp K^\pm$ pairs from proton-nucleus collisions are produced either directly or originate from short-lived (e.g., Δ, ρ), medium-lived (e.g., ω, ϕ), or long-lived (e.g., η', η) sources. Pion-kaon pairs produced directly, from short- or medium-lived sources, undergo Coulomb FSI resulting in modified unbound states (Coulomb pair in Fig. 1) or even forming bound systems in S states with a known distribution of the principal quantum number [18] ($A_{K\pi}$ in Fig. 1). Pairs from long-lived sources are practically not affected by the Coulomb interaction (non-Coulomb pair in Fig. 1). The accidental pairs are generated via different proton-nucleus interactions. The $\pi^\mp K^\pm$ Coulomb pair production is described in the pointlike production approximation by

$$\frac{d^2\sigma_C}{d\vec{p}_K d\vec{p}_\pi} = \frac{d^2\sigma_s^0}{d\vec{p}_K d\vec{p}_\pi} \times A_C(q) \quad \text{with}$$
$$A_C(q) = \frac{4\pi p_B/q}{1 - \exp(-4\pi p_B/q)}, \tag{1}$$

where the inclusive production cross section of πK pairs from short-lived sources without FSI is denoted by σ_s^0, the Coulomb enhancement function $A_C(q)$ is the Gamow factor [21–23], p_B is the Bohr momentum, and q the relative momentum in the pair c.m. system at the point of production. The distribution of the πK atom momentum is the same as for Coulomb pairs. For π and K production from nonpointlike medium-lived sources, corrections at the percent level were applied to the production cross sections [24]. Strong final state elastic and inelastic interactions are negligible [24].

Data processing.—Only events with one or two particle tracks in the DC detector of each arm are processed. The event reconstruction is performed according to the following steps. 1. One or two hadron tracks are identified in the DC of each arm with hits in the VH, HH, and preshower slabs and no signal in the ChN and the two-layer muon scintillation counter. 2. Track segments, reconstructed in the DC, are extrapolated backward to the beam position in the target, using the transfer function of the dipole magnet and the DIRAC reconstruction program ARIANE. This procedure provides approximate particle momenta and the corresponding points of intersection in the MDC, SFD, and IH. 3. Hits are searched for around the expected SFD coordinates in the region ± 1 cm, corresponding to $(3\text{–}5)\sigma_{\mathrm{pos}}$ defined by the position accuracy, taking into account the particle momenta. The number of hits around the two tracks is ≤ 4 in each SFD plane and ≤ 9 in all three SFD planes. The case of only one hit in the region ± 1 cm can occur because of detector inefficiency (two crossing particles, but one is not detected) or if two particles cross the same SFD column. The latter type of event may be recovered by selecting double ionization in the corresponding IH slab. For the data collected in 2007 with the Pt target, the criteria are different: the number of hits is two in the Y and U plane (signals from the SFD X plane and IH, which may resolve the crossing of only one SFD column by two particles, were not available in 2007). The momentum of the positively or negatively charged particle is refined to match the X coordinates of the DC tracks as well as the SFD hits in the X or U plane, depending on the presence of hits. In order to find the best two-track combination, the two tracks may not use a common SFD hit in the case of more than one hit in the proper region. In the final analysis, the combination with the best χ^2 in the other SFD planes is kept.

In order to improve the setup alignment, the decays of the Λ and $\bar{\Lambda}$ particles into $p\pi^-$ and $\pi^+\bar{p}$ are exploited [3,25]. By requiring the mass equalities $M_\Lambda^{\mathrm{expt}} = M_{\bar{\Lambda}}^{\mathrm{expt}}$ and $M_\Lambda^{\mathrm{expt}} = M_\Lambda^{\mathrm{PDG}}$, the angles of the DC axes are modified by a few 10^{-4} rad. The Λ mass width in the simulated distribution tests how well the MC simulation reproduces the momentum and angle resolution. The experimental Λ mass width, obtained in 2008–2010, differs from the simulation by (0.3–0.4)%. This difference can be removed by introducing a Gaussian smearing of the reconstructed momenta [3]. Considering this smearing, the momentum resolution varies from 2.8×10^{-3} to 4.4×10^{-3} for particle momenta

from 1.5 and 8 GeV/c [3]. The following resolutions of the relative momentum after the target are found: $\sigma_{QX} \approx \sigma_{QY} \approx 0.36$ MeV/c, $\sigma_{QL} \approx 0.94$ MeV/c for $p_{\pi K} = p_\pi + p_K = 5$ GeV/c, and about 6% worse values for $p_{\pi K} = 7.5$ GeV/c.

Selected events are classified into three categories: $\pi^- K^+$, $\pi^+ K^-$, and $\pi^- \pi^+$. The last category is used for calibrating purposes. Pairs of πK are cleaned of $\pi^- \pi^+$ and $\pi^- p$ background by the Cherenkov counters ChF and ChA (see the section "Setup"). In the momentum range from 3.8 to 7 GeV/c, pions are detected by the ChF with (95–97)% efficiency [26], whereas kaons and protons (antiprotons) do not produce any signal. The admixture of $\pi^- p$ pairs is suppressed by the ChA, which records kaons but not protons [27]. Because of the finite detector efficiency, a certain admixture of misidentified pairs still remains in the experimental distributions. For the selected events, the applied procedure plots the distribution of the measured difference ΔT of particle generation times. These times of production at the target are the times measured by the VH and reduced by the time-of-flight from the target to the VH planes for particles with the expected masses ($K^\pm$ and $\pi^\mp$ mesons) and the measured lab momenta. For $\pi^- K^+$ ($\pi^+ K^-$) pairs, the difference is centered at 0, and for misidentified pairs, biased. Figure 3 presents the distribution of the difference of the particle production times for K^+ mesons in the range (4.4–4.5) GeV/c. The distribution is fitted by the simulated distribution of the admixed fractions. The contribution of misidentified pairs was estimated and accordingly subtracted [28]. Figure 4 shows, after applying the selection criteria, the well-defined $\pi^- K^+$ Coulomb peak at $Q_L = 0$ and the strongly suppressed peak from Λ decays at $Q_L = -30$ MeV/c. The Q_L distribution of $\pi^+ K^-$ pairs is similar [3].

Analysis and results.—Since the samples of πK data consist of Coulomb, non-Coulomb, and atomic pairs, these event types were generated by MC [DIPGEN [29], GEANT-DIRAC (setup simulator)] simulations. The non-Coulomb pairs are distributed in accordance with the phase space, while the q distribution of Coulomb pairs is modified by the factor $A_C(q)$ (1). The MC simulation provides the lab momentum distributions for the Coulomb and non-Coulomb pairs [29]. The sum of these pair distributions is fitted to the corresponding experimental distributions. The simulation of atomic pairs includes the position of the breakup point, the quantum numbers of the atomic state, and the q distribution of the resulting atomic pairs. The evaluation is done by solving numerically the transport equations [30] using the total and transition cross sections [31]. The description of the charged particle propagation through the setup takes into account (a) multiple scattering in the target, detector planes, and setup partitions, (b) the response of all detectors, (c) additional momentum smearing, and (d) the results of the SFD response analysis [28,32,33] with the influence on the Q_T resolution. The same theoretical approach and reconstruction procedure provide a good description of about 21 000 $\pi^+ \pi^-$ atomic pairs in the Q_L and Q_T distributions [10].

In the analysis of the πK data, the experimental one-dimensional distributions of the relative momentum Q and $|Q_L|$ and the two-dimensional distributions ($|Q_L|$, Q_T) were fitted for each year and each combination of πK charges by simulated distributions of atomic, Coulomb, and non-Coulomb pairs. Their corresponding numbers n_A, N_C, and N_{nC} are free fit parameters. The sum of these

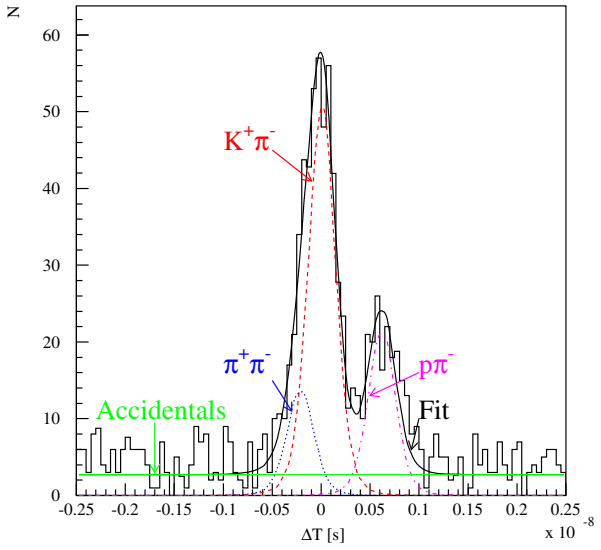

FIG. 3. Difference of particle generation times for events with positively charged particle momenta (4.4–4.5) GeV/c. Experimental data (histogram) are fitted by the event sum (black, solid): $K^+\pi^-$ (red, dashed), $\pi^+\pi^-$ (blue, dotted), $p\pi^-$ (magenta, dotted dashed), and accidentals (green, constant).

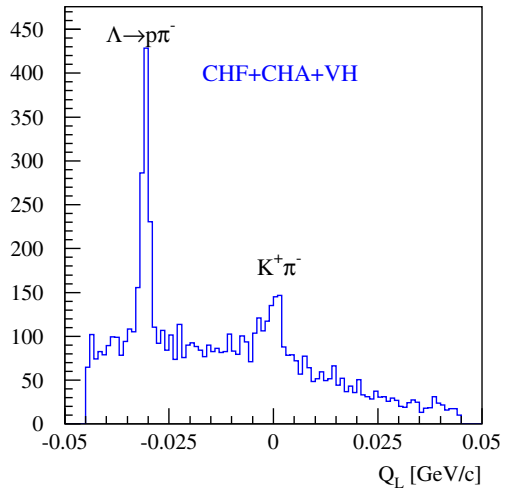

FIG. 4. Q_L distributions of potential $\pi^- K^+$ pairs after applying the selection as described in the text. Events with positive Q_L are suppressed compared to those with negative Q_L due to the lower acceptance and lower production cross section.

parameters is equal to the number of analysed events. The fitting procedure took into account the statistical errors in the experimental and the MC distribution—the latter is more than 1 order less than the experimental one.

The experimental and simulated Q distributions of the π^-K^+ and π^+K^- pairs are shown in Fig. 5 (top) for all events with $Q_T < 4$ MeV/c and $|Q_L| < 20$ MeV/c. One observes an excess of events above the sum of Coulomb and non-Coulomb pairs in the low Q region, where atomic pairs are expected. After background subtraction there is a signal at the level of 5.7σ, shown in Fig. 5 (bottom): $n_A = 349 \pm 61$ ($\chi^2/n = 41/37$, n = number of degrees of freedom). The signal shape is described by the simulated distribution of atomic pairs. The numbers of atomic pairs, produced in the Ni and Pt targets, are $n_A(\mathrm{Ni}) = 275 \pm 57$ ($\chi^2/n = 40/37$) and $n_A(\mathrm{Pt}) = 73 \pm 22$ ($\chi^2/n = 40/36$), respectively. The same analysis was performed for the π^-K^+ and π^+K^- pairs separately. The numbers of π^-K^+ and π^+K^- atomic pairs are $n_A = 243 \pm 51$ ($\chi^2/n = 36/37$) and $n_A = 106 \pm 32$ ($\chi^2/n = 42/37$), respectively. The experimental ratio (2.3 ± 0.9) between the two types of atom production, corrected by the difference of their detection efficiencies, equals 2.7 ± 1.1, compatible with the ratio 2.4 as calculated using FRITIOF [34]. In the two-dimensional ($|Q_L|$,Q_T) analysis, all experimental data were analysed in the same $|Q_L|$ and Q_T intervals using simulated two-dimensional distributions. The evaluated number of atomic pairs, $n_A = 314 \pm 59$ ($\chi^2/n = 237/157$), corresponds to 5.3σ and coincides with the result of the previous analysis. In Table I, the results of the three types of analysis (Ni and Pt target together) are presented for each atom type and combined. There is good agreement between the results of the Q and ($|Q_L|$,Q_T) analyses. The one-dimensional $|Q_L|$ analysis for all πK data yields $n_A = 230 \pm 92$ ($\chi^2/n = 52/37$), which does not contradict the values obtained in the other two statistically more precise analyses.

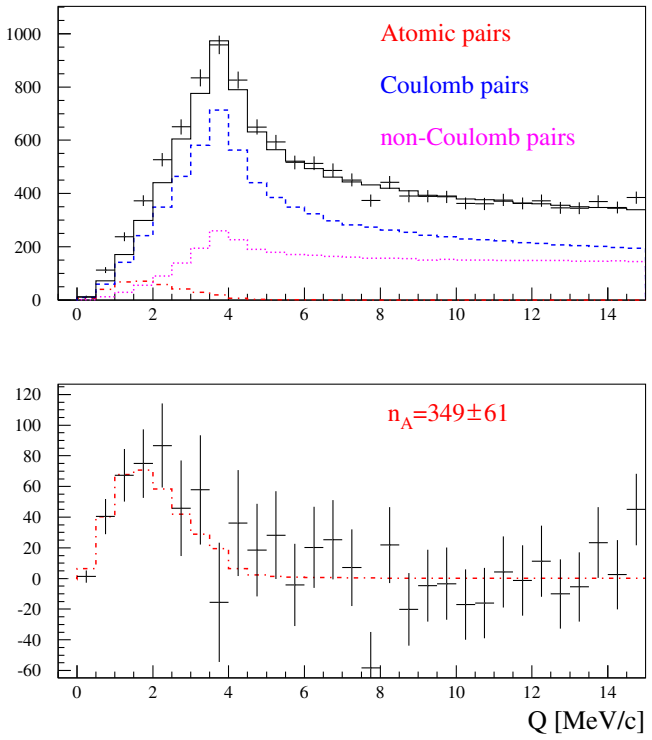

FIG. 5. Top: Q distribution of the experimental π^-K^+ and π^+K^- pairs fitted by the sum of the simulated distributions of atomic (red, dotted dashed), Coulomb (blue, dashed), and non-Coulomb pairs (magenta, dotted). Free (Coulomb and non-Coulomb) pairs are shown as black and solid line. Bottom: difference distribution between the experimental and simulated free pair distributions compared with the simulated atomic pairs. The number of observed atomic pairs is denoted by n_A.

Compared to the previous investigation [1], the Pt data were analysed including the upstream detectors. The consequence is a decrease of the statistics, but on the other hand an increase of the Q_T resolution. This better resolution improves the quality of the data. Concerning the Ni target, the increase of n_A, compared to Ref. [3], is caused by optimizing the time-of-flight criteria, which decreases the atomic pair losses for the same fraction of background in the final distributions.

The evaluation of the atomic pair number n_A is affected by several sources of systematic errors [25,28]: the uncertainty of the Λ width correction, the uncertainty of the multiple scattering in the Ni and Pt targets, the uncertainty of the SFD simulation, the uncertainty of the lab momentum spectrum for the πK and background pairs, and the correction of the Coulomb correlation function on the finite size region of production. These uncertainties lead to differences in the shapes of the experimental and MC distributions for the atomic, for the Coulomb, and, to a much lesser extent, for the non-Coulomb pairs. The shape differences induce a bias in the value of the fit parameter n_A, corresponding to a systematic error of the atomic pair number. The values of the induced systematic errors were estimated [28] by describing the experimental data with some distributions simulated with varied setup properties. This method gives the sensitivity of the uncertainty of the different parameters. The values of the uncertainties were estimated by separate measurements [25,28]. In total, one gets an estimation of the systematic errors. The total systematic errors for the Q, ($|Q_L|$, Q_T), and Q_L analyses are 8.6, 10.1, and 6.4, respectively.

TABLE I. Atomic pair numbers n_A by analysing the one-dimensional Q and $|Q_L|$ distributions and the two-dimensional ($|Q_L|$,Q_T) distribution. Only statistical errors are given.

Analysis	π^-K^+	π^+K^-	π^-K^+ and π^+K^-
Q	243 ± 51 (4.7σ)	106 ± 32 (3.3σ)	349 ± 61 (5.7σ)
$\lvert Q_L\rvert$	164 ± 79 (2.1σ)	67 ± 47 (1.4σ)	230 ± 92 (2.5σ)
$\lvert Q_L\rvert, Q_T$	237 ± 50 (4.7σ)	78 ± 32 (2.5σ)	314 ± 59 (5.3σ)

Conclusion.—In the DIRAC experiment at CERN, the dimesonic Coulomb bound states involving strangeness, the $\pi^- K^+$ and $\pi^+ K^-$ atoms, were observed for the first time with reliable statistics. These atoms are generated by a 24 GeV/c proton beam hitting Pt and Ni targets. In the same targets, a fraction of the produced atoms breaks up, leading to $\pi^- K^+$ and $\pi^+ K^-$ atomic pairs with small relative momenta Q. The one-dimensional $\pi^\mp K^\pm$ analysis in Q yields $349 \pm 61(\text{stat}) \pm 9(\text{syst}) = 349 \pm 62(\text{tot})$ atomic pairs (5.6σ) for both combinations of charge. Analogously, a two-dimensional analysis in ($|Q_L|$, Q_T) was performed with the result of $314 \pm 59(\text{stat}) \pm 10(\text{syst}) = 314 \pm 60(\text{tot})$ atomic pairs (5.2σ), in agreement with the former number.

The resulting πK atom lifetime and πK scattering length from the ongoing analysis will be presented in a separate paper.

We are grateful to R. Steerenberg and the CERN PS accelerator crew for the delivery of a high quality proton beam and the permanent effort to improve the beam characteristics. The project DIRAC has been supported by the CERN and JINR administrations, the Ministry of Education and Youth of the Czech Republic by Project No. LG130131, the Istituto Nazionale di Fisica Nucleare and the University of Messina (Italy), a Grant-in-Aid for Scientific Research from the Japan Society for the Promotion of Science, the Ministry of Education and Research (Romania), the Ministry of Education and Science of the Russian Federation and the Russian Foundation for Basic Research, the Dirección Xeral de Investigación, Desenvolvemento e Innovación, Xunta de Galicia (Spain), and the Swiss National Science Foundation.

*Corresponding author
juerg.schacher@cern.ch

[1] B. Adeva *et al.*, Phys. Lett. B **674**, 11 (2009).
[2] Y. Allkofer, Ph.D. thesis, Universität Zürich, 2008.
[3] B. Adeva *et al.*, Phys. Lett. B **735**, 288 (2014).
[4] S. Weinberg, Phys. Rev. Lett. **17**, 616 (1966).
[5] J. Gasser and H. Leutwyler, Nucl. Phys. **B250**, 465 (1985).
[6] B. Moussallam, Eur. Phys. J. C **14**, 111 (2000).
[7] G. Colangelo, J. Gasser, and H. Leutwyler, Nucl. Phys. **B603**, 125 (2001).
[8] L. Afanasyev *et al.*, Phys. Lett. B **308**, 200 (1993).
[9] B. Adeva *et al.*, Phys. Lett. B **619**, 50 (2005).
[10] B. Adeva *et al.*, Phys. Lett. B **704**, 24 (2011).
[11] S. M. Bilen'kii *et al.*, Yad. Fiz. **10**, 812 (1969) [Sov. J. Nucl. Phys. **10**, 469 (1969)].
[12] J. Schweizer, Phys. Lett. B **587**, 33 (2004).
[13] V. Bernard, N. Kaiser, and Ulf.-G. Meissner, Phys. Rev. D **43**, R2757 (1991); Nucl. Phys. **B357**, 129 (1991).
[14] B. Kubis and U. G. Meissner, Phys. Lett. B **529**, 69 (2002).
[15] J. Bijnens, P. Dhonte, and P. Talavera, J. High Energy Phys. 05 (2004) 036.
[16] P. Buettiker, S. Descotes-Genon, and B. Moussallam, Eur. Phys. J. C **33**, 409 (2004).
[17] K. Sasaki, N. Ishizuka, M. Oka, and T. Yamazaki, Phys. Rev. D **89**, 054502 (2014).
[18] L. Nemenov, Yad. Fiz. **41**, 980 (1985) [Sov. J. Nucl. Phys. **41**, 629 (1985)].
[19] B. Adeva *et al.*, Phys. Lett. B **751**, 12 (2015).
[20] O. Gorchakov and A. Kuptsov, Report No. DN-2005-05; cds.cern.ch/record/1369686.
[21] A. Sommerfeld, *Atombau und Spektrallinien* (F. Vieweg & Sohn, Braunschweig, 1931).
[22] G. Gamow, Z. Phys. **51**, 204 (1928).
[23] A. Sakharov, Zh. Eksp. Teor. Fiz. **18**, 631 (1948); Sov. Phys. Usp. **34**, 375 (1991).
[24] R. Lednicky, J. Phys. G **35**, 125109 (2008).
[25] A. Benelli and V. Yazkov, Report No. DN-2016-01; cds.cern.ch/record/2137645.
[26] P. Doskarova and V. Yazkov, Report No. DN-2013-05; cds.cern.ch/record/1628541.
[27] A. Benelli and V. Yazkov, Report No. DN-2009-07; cds.cern.ch/record/1369628.
[28] V. Yazkov and M. Zhabitsky, Report No. DN-2013-06; cds.cern.ch/record/1628544.
[29] DIRAC Collaboration, Report No. CERN-EP-2016-128; arXiv:1605.06103.
[30] M. Zhabitsky, Phys. At. Nucl. **71**, 1040 (2008).
[31] L. Afanasyev and A. Tarasov, Phys. At. Nucl. **59**, 2130 (1996).
[32] A. Gorin, S. Horikawa, K. Kuroda, I. Manuilov, K. Okada, A. Ryazantsev, A. Sidorov, and F. Takeutchi, Nucl. Instrum. Methods Phys. Res., Sect. A **566**, 500 (2006).
[33] A. Benelli, SFD study and simulation for the data 2008-2010, Report No. DIRAC-TALK-2011-01.
[34] O. Gorchakov and L. Nemenov, JPhysG-101308.R1.